Carbon 170 (2020) 137–145

Contents lists available at ScienceDirect

Carbon

journal homepage: www.elsevier.com/locate/carbon

Research Article

Photoexcited state properties and antibacterial activities of carbon dots relevant to mechanistic features and implications

Xiuli Dong [a], Lin Ge [b], Dina I. Abu Rabe [a], Oluwayemisi O. Mohammed [a], Ping Wang [b], Yongan Tang [c], Sophia Kathariou [d], Liju Yang [a, **], Ya-Ping Sun [b, *]

[a] Department of Pharmaceutical Sciences, Biomanufacturing Research Institute and Technology Enterprise, North Carolina Central University, Durham, NC, 27707, USA
[b] Department of Chemistry and Laboratory for Emerging Materials and Technology, Clemson University, Clemson, SC, 29634, USA
[c] Department of Mathematics and Physics, North Carolina Central University, Durham, NC, 27707, USA
[d] Department of Food, Bioprocessing & Nutrition Sciences, North Carolina State University, Raleigh, NC, 27695, USA

ARTICLE INFO

Article history:
Received 30 June 2020
Received in revised form
20 July 2020
Accepted 9 August 2020
Available online 15 August 2020

Keywords:
Carbon dots
Antibacterial
Light activation
Redox species
Photodynamic
Mechanism

ABSTRACT

Carbon dots (CDots) are strongly absorptive over the visible spectrum, with the effective photon-harvesting driving rich excited state processes and properties. In this work, spectroscopic probing of these processes and properties is coupled with the evaluation of the photoinduced bactericidal function of CDots, aimed toward making correlations among the findings from the former and those from the latter on the inactivation of bacterial pathogens. Within the general mechanistic framework for CDots, the observed effective and efficient antibacterial activities of the CDots under visible light are attributed to major contributions by the initially photo-generated electrons and holes that are trapped at passivated surface defect sites of the dots, in addition to the traditional reactive oxygen species (ROS) produced in the emissive excited states from the recombination of the redox pairs. Such major contributions to the inactivation of the bacteria by the separated redox species in CDots can not be quenched by ROS scavengers commonly used in the study of photodynamic effects with classical molecular photosensitizers, thus making light-activated CDots uniquely potent antimicrobial agents. The characteristic features of photoexcited CDots and their related mechanistic implications are discussed in reference to the similar behaviors and mechanistic model of conventional semiconductor quantum dots.

1. Introduction

Carbon dots (CDots) [1–3], or in some literature reports also dubbed “carbon quantum dots” for some of their properties similar to those found in conventional semiconductor quantum dots (QDs), have attracted much recent attention [3–14]. As the “dots” based on or derived from carbon, their core structures are small carbon nanoparticles (Fig. 1). These nanoparticles, representing nanoscale carbon allotrope at the zero-dimension [3,15], are of unique characteristics, especially in terms of optical and redox properties [16]. Such properties can be dramatically enhanced by the various passivation schemes targeting the nanoparticle surface defects, with the most effective being the surface chemical functionalization with selected organic species to result in CDots (Fig. 1) of bright and colorful fluorescence emissions and other photoexcited state processes and properties.

CDots due to the core carbon nanoparticles are strongly absorptive in the visible, extending into the near-IR [9,17], as the organic molecules selected generally or purposely for the nanoparticle surface functionalization are transparent in the same spectral regions. However, the photoexcited state processes and properties of CDots are mostly different from those of the core carbon nanoparticles, as a result of the nanoparticle surface passivation-functionalization (Fig. 1). In fact, as suggested by the growing experimental evidence, many behaviors of photoexcited CDots are phenomenologically and to a significant extent mechanistically similar to those of conventional semiconductor QDs [3,16]. These similarities, beyond the observed strong and multicolor fluorescence emissions, have been reflected by or driving their comparable uses in optoelectronics and related technologies [16], including various components or functions in photovoltaic

* Corresponding author.
** Corresponding author.
E-mail addresses: lyang@nccu.edu (L. Yang), syaping@clemson.edu (Y.-P. Sun).

https://doi.org/10.1016/j.carbon.2020.08.025
0008-6223/

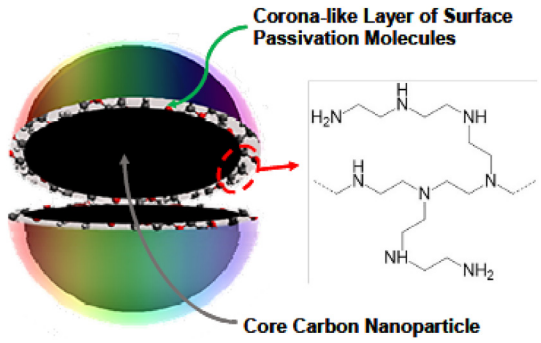

Fig. 1. A cartoon illustration on the structure in CDots in general, with the branched polyethylenimine oligomer (PEI) as surface functionalization molecule highlighted for PEI-CDots specifically. (A colour version of this figure can be viewed online.)

devices, light-emitting diodes, and photocatalytic systems [18–22].

As related to the photocatalytic characteristics, CDots, again similar to nanoscale semiconductors, have been demonstrated for their effective light-activated antimicrobial activities [14]. For example, in an early study CDots under visible/natural light were found to be able to effectively inactivate *E. coli* cells both in suspension and on surface [23]. Since then, the photoinduced antibacterial activities of CDots have been correlated empirically with their fluorescence emission parameters, quantum yields in particular [24], offering a glimpse into the mechanistic implications and complexities. On the other hand, similarly experimental observations-based correlations have been made between the antimicrobial outcomes and the structural features of CDots, including especially the dot surface functionalities [25] or chemical compositions of those dot samples produced by various carbonization syntheses from organic precursors [14,26–30].

The light-activated antimicrobial functions of CDots are apparently driven by and correlated with their photoexcited states and related redox processes and species, thus logically a part of the general mechanistic framework for these carbon nanomaterials [3]. In the work reported here our effort was to make some connections among the optical spectroscopy results reflecting the photoexcited state properties of the selected CDots and the results on their visible light-driven effective and efficient inactivation of several bacterial pathogen strains, for the mechanistic relevance and insights.

2. Experimental section

2.1. Materials

The carbon nanopowder sample (US1074) was acquired from US Research Nanomaterials, Inc. Oligomeric polyethylenimine (PEI, average molecular weight ~600, branched) was purchased from Polysciences, and *N*,*N*-diethylaniline (DEA) and 2,4-dinitrotoluene (DNT) from Sigma-Aldrich. Dialysis membrane tubing was supplied by Spectrum Laboratories. Water was deionized and purified by being passed through a Labconco WaterPros water purification system.

2.2. Measurement

UV/vis absorption spectra were recorded on Shimadzu UV2501 and UV-3600 spectrophotometers. Fluorescence spectra were measured on a Jobin-Yvon emission spectrometer equipped with a 450 W xenon source, Gemini-180 excitation and Triax-550 emission monochromators, and a photon counting detector (Hamamatsu R928P PMT at 950 V). The as-measured spectra were corrected for nonlinear instrument response by using predetermined correction factors. Fluorescence quantum yields were determined by using the relative method with 9,10-bis(phenylethynyl)-anthracene in cyclohexane as a standard. Fluorescence decays were measured by using the time-correlated single photon counting (TCSPC) technique on a Horiba Ultima Extreme spectrometer equipped with a SuperK Extreme supercontinuum laser source pulsed at 10 MHz, TDM-800 excitation and TDM-1200 emission monochromators, a R3809-50-MCP-PMT detector operated at 3 kV in a thermoelectrically cooled housing, and FluoroHub A++ timing electronics. Experimental decay curves were deconvoluted by using the Das6 decay analysis software. Transmission electron microscopy (TEM) imaging was performed on a Hitachi H-9500 high-resolution TEM system.

2.3. PEI-CDots

The small carbon nanoparticles were harvested from the commercially acquired carbon nanopowder sample in the procedure reported previously [31]. The nanoparticles were used for the functionalization with PEI in the microwave-assisted thermal reaction. Briefly, the nanoparticle sample (100 mg) as an aqueous slurry was mixed with PEI (2 g) and ethanol (2 mL) in a scintillation vial with sonication in an ultrasonic cleaner (VWR 250D), followed by solvent evaporation for a solid mixture. Separately, a silicon carbide (150 g) bath in silica crucible casting dish (about 8 cm in diameter and 2.5 cm in height) was pre-heated in a conventional microwave oven at 500 W for 3 min. Then, several rounds of microwave heating were as follows: (1) the vial containing the solid mixture was immersed in the pre-heated silicon carbide bath for microwave irradiation at 1000 W for 3 min; (2) the sample vial was taken out of the bath and cooled to the ambient, and more PEI (1 g) and ethanol (2 mL) were added to the sample and mixed well, followed by the solvent evaporation and then microwave irradiation the same as in (1); (3) a repeat of (2) but with the microwave irradiation at 500 W for 8 min; and (4) a repeat of (3). The final reaction mixture was cooled to ambient and dispersed in deionized water with vigorous sonication. The resulting aqueous dispersion was centrifuged at 5000 *g* to collect the supernatant, followed by dialysis (molecular weight cut-off ~1000) against fresh water for 6 h to obtain PEI-CDots in an aqueous solution.

2.4. Bacterial strains and cultures

The pathogenic *Enterococcus spp.* strains 9144, 9756, and *Enterococcus faecium* BM46 were used in this study. These strains were isolated from poultry processing plants and animal productions, and they were found in test results to be resistant to multiple antibiotics, including for example tetracycline, erythromycin, and nalidixic acid (see Supplementary Material).

Bacterial cultures were grown in 15 mL brain heart infusion (BHI) broth (Oxoid, UK) by inoculating the broth with a single colony from BHI agar plates, and incubated overnight at 37 °C with constant agitation at 225 rpm in an Excella E24 incubator shaker (New Brunswick Scientific, Edison, NJ, USA). Bacterial cultures were centrifuged at 12,000 *g* (Beckman Coulter Life Sciences, Indianapolis, IN, USA) for 8 min and washed twice using phosphate buffer saline (PBS). The pellet was then re-suspended in PBS and used in further experiments. The actual cell numbers in the cultures were determined using the traditional agar surface plating method.

2.5. Treatment of bacterial cells with PEI-CDots under visible light

Aliquots (100 μL) of the bacterial cell suspension were placed

into the wells of a 96-well plate at the concentration of ~10^7–10^8 CFU/mL, then 100 μL of PEI-CDots at desired concentrations were added to the wells to reach the final dot concentrations of 0.025, 0.062, 0.12, 0.25, and 0.62 μM_{CDOTS} (where M_{CDOTS} denotes the molar concentration of the dots). The plates were placed on a shaker (BT Lab Systems, St Louis, MO, USA) at 350 rpm, and exposed to visible light from a household LED lamp (Cree, 10 W, 5000K) placed at ~10 cm above the plate (observed light intensity at the plate ~4.8 mW/cm^2) for the selected time duration. Unless specified otherwise, the same light source and conditions were used in all antibacterial experiments. Samples without CDots and those with CDots but in dark were used as the controls. After the treatment, the viable cell numbers in the treated and control samples were determined using the traditional plating method for the evaluation of the bactericidal effect.

2.6. Intracellular ROS level and scavenging

Bacterial cells were collected after overnight growth by centrifugation at 12,000 *g* for 8 min. The pellets were washed twice with 0.85% NaCl and re-suspended in 5 mL of 0.85% NaCl. The cells were treated with PEI-CDots under visible light in the same setup described above. After the treatment, the cells were collected and washed twice with 800 μL of 0.85% NaCl, and the pellets were re-suspended in 350 μL 0.85% NaCl. Aliquots (200 μL each) of 10 μM solution of the fluorescence probe dihydrorhodamine 123 (DHR 123) were added to the samples and then vigorously vortexed. After 40 min incubation in the dark at room temperature, the cells were washed twice and re-suspended in 350 μL of 0.85% NaCl. The fluorescence at 535 nm in each well was measured using a SpectraMax M5 microplate reader (Molecular Devices, San Jose, CA, USA) with excitation at 500 nm. Using the fluorescence intensities of the controls as the 100% baseline, the percentages of increased intracellular ROS levels in the CDots treated samples were calculated by using the measured fluorescence intensities of the treated samples in reference to those of the controls.

The same experiments above were performed with the presence of 30 mM L-histidine or *t*-butanol in the treatments under otherwise the same experimental conditions for an evaluation on their scavenging ability to reduce the intracellular ROS levels.

2.7. Lipid peroxidation

The TBARS assay kit purchased from Cell Biolabs was used to quantify malondialdehyde (MDA), one of the products in lipid peroxidation. Samples of bacterial cells post-treatment with PEI-CDots under visible light were centrifuged at 9000 *g* (Beckman Coulter Life Sciences, Indianapolis, IN, USA) for 7 min. The cells were washed once with PBS, and the pellets were re-suspended in 200 μL PBS. An aliquot of 2 μL of 100 × butylated hydroxytoluene (100 × BHT) was added to the sample to prevent any further oxidation. Then, 100 μL of each treated sample, the control, and the malondialdehyde (MDA) standard (from the TBARS assay kit) were transferred to 1.5 mL microcentrifuge tubes, followed by the addition of 100 μL aliquot of SDS lysis solution. All of the samples were mixed thoroughly and incubated at room temperature for 5 min. Then, to each of the treated samples, controls, and MDA standards was added 250 μL aliquot of the TBA reagent. After the incubation at 95 °C for 50 min, the samples were allowed to cool down to room temperature by placing them in an ice bath for 5 min. All of the samples were centrifuged at 1000 *g* for 15 min, and an aliquot (200 μL) of the supernatant of each sample was loaded to the wells of a 96-well plate for measuring the absorbance at 532 nm with the SpectraMax M5 microplate reader. The absorbances at 532 nm of the treated and control samples were used to calculate the quantity of MDA using the standard curve generated with the MDA standards in the same experiment.

2.8. Membrane permeability tests

Samples of BM46 cells post-treatment with PEI-CDots under visible light were centrifuged and re-suspended in 50 μL 0.85% NaCl, and to the bacterial suspensions were each added 5 μL of the Live/Dead Baclight™ bacterial viability kit (Invitrogen, Eugene, OR). Upon mixing thoroughly, the mixtures were incubated in the dark at room temperature for 15 min. Then, fluorescent images of the treated and untreated cells were taken under a Nikon Eclipse E600FN fluorescence microscope (Japan).

2.9. Statistical analysis

All measurements were performed at least four replicates in two independent experiments. Experimental results were presented as the mean of the replicates with standard deviation. Significant differences between the experimental results were assessed using the general linear model (GLM) procedure of the SAS System 9.2 (SAS Institute Inc., Cary, NC, USA), with $P \leq 0.05$ considered as significant different.

3. Results and discussion

Pre-processed and selected small carbon nanoparticles of around 5 nm in diameter were functionalized by oligomeric polyethylenimine (PEI, average molecular weight ~600) in microwave-assisted thermal reactions to obtain the targeted PEI-CDots (Fig. 1). These CDots are readily soluble in water and polar organic solvents for colored solutions. Their optical absorptions (Fig. 2) are largely the same as those of the same carbon nanoparticles before the PEI functionalization. For the nanoparticles, the estimated optical absorptivity at 400 nm is 50–100 (averaging 75) $M_C^{-1}cm^{-1}$, where M_C is the molar concentration of carbon atoms in the solution. For CDots, there has been no experimental evidence suggesting any significant changes in optical absorptivity from that of the core carbon nanoparticles due to the particle surface passivation-functionalization. Thus, the estimated optical absorptivity for CDots of core carbon nanoparticles averaging 5 nm in diameter is ~5×10^5 $M_{DOTS}^{-1}cm^{-1}$ at 400 nm, where M_{DOTS} denotes molar concentration of the dots in solution.

Upon photoexcitation, CDots are known to exhibit bright and

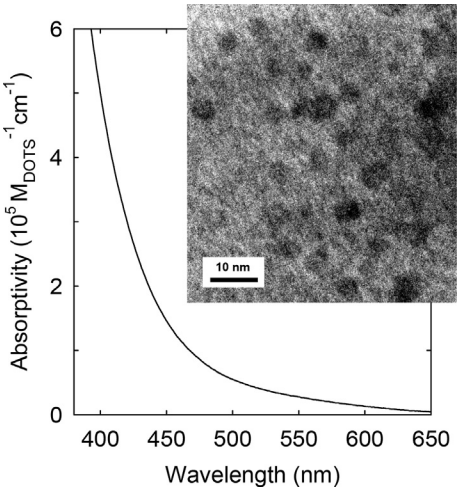

Fig. 2. Optical absorptions in solution and TEM images (inset) of PEI-CDots.

colorful fluorescence emissions, for which PEI-CDots are obviously no exception and also show the same characteristic excitation wavelength dependencies for both fluorescence spectra and quantum yields (Fig. 3) [32]. The consistency in such dependencies represents a strong evidence for their well defined mechanistic origins [3].

In the mechanistic framework for CDots, which is generally consistent with or supported by the available experimental results [3,9,32], the photoexcitation is into the core carbon nanoparticles for their being responsible for the photon-harvesting because the surface organic functionalization molecules/species are completely transparent at the excitation wavelengths. Due to some intrinsic electronic features of the photoexcited carbon nanoparticles, on which little is known theoretically, the photoexcitation must be triggering the rapid charge transfer and separation for the formation of electrons and holes, which are likely trapped at various surface defect sites. The chemical functionalization of the carbon nanoparticles in CDots is thought to provide surface passivation to stabilize the defect sites [31]. Experimentally, there have been some ultrafast pump-probe spectroscopy results on CDots [33,34] suggesting strong and broad transient absorptions with rise time on the sub-picosecond time scale (including also the results shared by Profs. Susanne Ullrich and Yiping Zhao at University of Georgia, USA), which could be associated with the proposed separated redox pairs. At a longer time scale in nanoseconds are the characteristic fluorescence emissions, which could be detected in solvent suspensions of small carbon nanoparticles [17,31], but are orders of magnitude stronger in CDots due to the effective surface passivation via chemical functionalization of the nanoparticles [31]. The presence of two regimes on two vastly different time scales in photoexcited CDots has been used in the rationalization of the consistently observed characteristic excitation wavelength dependencies of fluorescence emission spectra and quantum yields (Fig. 3), as well as fluorescence decays [32]. In such a framework for photoexcited states in CDots, there are apparently some features comparable with those in the exciton model for nanoscale semiconductors [35], and also some of the same or other features shared with organic dyes. However, of special interest are what and how

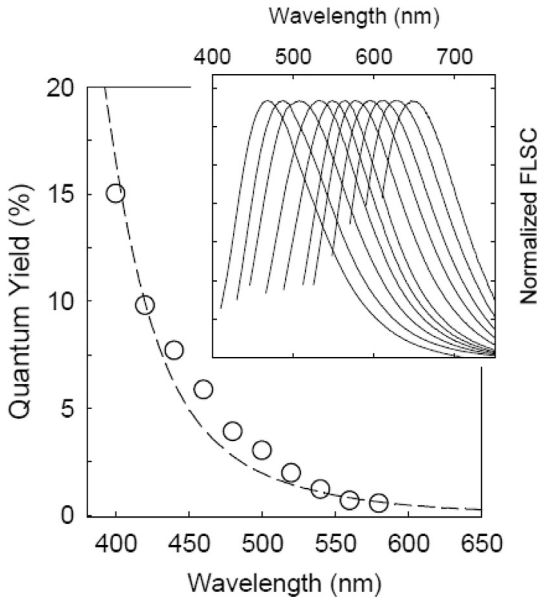

Fig. 3. Fluorescence (FLSC) quantum yields at different excitation wavelengths and spectra (inset, from left to right with excitation at 400 nm and in 20 nm increments) of PEI-CDots, with absorptions (- - -) also shown for comparison.

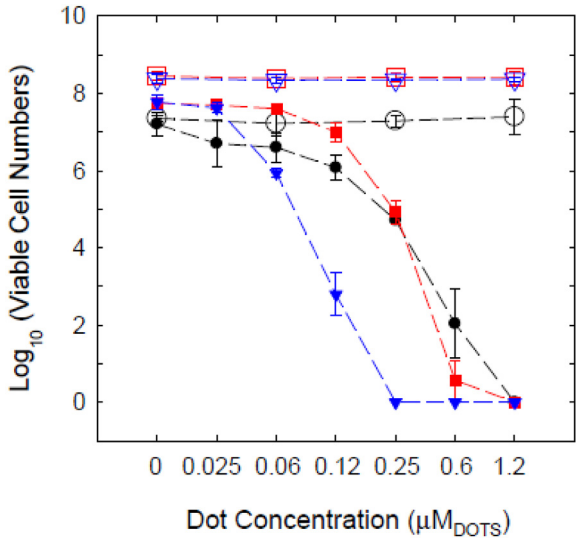

Fig. 4. Viable cell numbers (CFU/mL) in $\log_{10}$ scale for the cell samples (9144: triangle; 9756: square; BM46: circle) upon treatments with different concentrations of PEI-CDots under visible light for 1 h (solid symbols) and in dark (open symbols). (A colour version of this figure can be viewed online.)

these photoexcited state features contribute to or dictate the antimicrobial activities of CDots.

Experimentally, bacterial cells of *Enterococcus* strains 9144, 9755, and BM46 in PBS (10^7–10^8 CFU/mL) were treated with PEI-CDots at different concentrations up to 1.2 μM_{DOTS} under visible light for 1 h or in the dark as controls. As shown in Fig. 4, the treatment with PEI-CDots under visible light inactivated the bacterial cells effectively, as made evident by the reduced viable cell numbers *versus* those of the dark controls. The inactivation was obviously dot concentration dependent under the given experimental condition, with the complete inactivation (reduction > 7 logs) of cells in the samples achieved at 1.2 μM_{DOTS} for two strains and significantly lower dot concentration for the other one (Fig. 4). The inactivation was also dependent on the time of light exposure, more effective with a longer exposure time, such that the complete inactivation could be achieved at a lower dot concentration coupled with a longer visible-light exposure time (Fig. 5).

Among the three *Enterococcus* strains, the 9756 and BM46 strains are clearly more difficult than the 9144 strain in the inactivation by PEI-CDots with visible light, requiring a higher dot concentration and/or longer light exposure time for the same level of reduction in viable cell numbers (Figs. 4 and 5). Mechanically this could be due to biological factors such as their intrinsically different defense systems and resistance mechanisms. Biologically the inactivation by visible light-activated PEI-CDots was apparently associated with significant damages to the bacterial cells.

Often accompaning cell membrane damages is the lipid peroxidation [36], a process of multiple steps in which lipid carbon-carbon double bonds are attacked by free radicals and/or strong oxidants [37–39]. The lipid peroxidation produces lipid hydroperoxides (LOOH) and various aldehydes including especially malondialdehyde (MDA) [40,41], which is commonly used as an indicator for lipid peroxidation based on its reaction with thiobarbituric acid (TBA) to form a red fluorescent adduct [42–44]. In this study, the lipid peroxidation was analyzed by quantifying MDA with the thiobarbituric acid reactive substances assay (TBARS) [43,44]. As shown in Fig. 6, MDA levels in the cells treated by PEI-CDots with visible light are much higher than those in the controls, suggesting substantial lipid peroxidation in the treated cells.

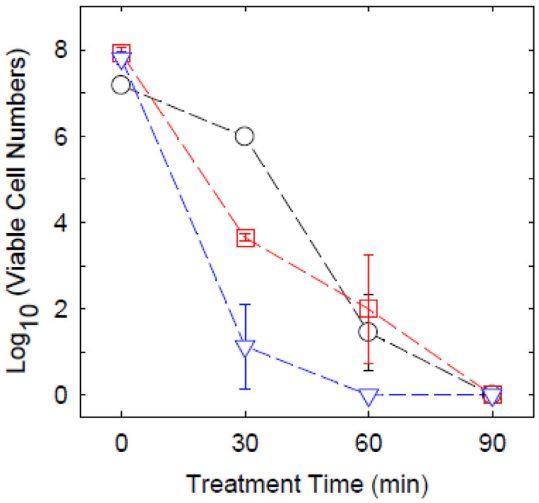

Fig. 5. Viable cell numbers (CFU/mL) in $\log_{10}$ scale for the cell samples (9144: triangle; 9756: square; BM46: circle) upon treatments with 0.6 μM_{DOTS} PEI-CDots under visible light for different periods of time. (A colour version of this figure can be viewed online.)

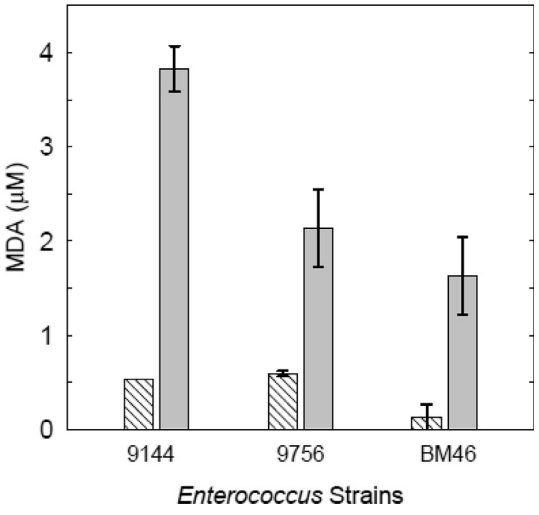

Fig. 6. Malondialdehyde (MDA) levels detected in different *Enterococcus* strains after the cells were treated with 1.2 μM_{DOTS} PEI-CDots under visible light for 1 h (grey bars) *versus* the controls (hatched bars).

The damages to the cell membrane can be assessed more directly with the live/dead bacterial viability kit, which contains two nucleic acid dyes to stain the live and dead cells for their significant differences in the membrane permeability. The green SYTO 9 dye can penetrate membranes of both live and dead cells, but the red propidium iodide (PI) dye can only penetrate the damaged cell membranes of dead cells. In this study, BM46 was selected as a representative example for the live/dead kit test. The BM46 cells treated with 1.2 μM_{DOTS} PEI-CDots for 1 h under visible light and the untreated controls were stained with the live/dead kit for examination under fluorescence microscope. As shown in Fig. 7, the BM46 cells in untreated controls are green (live and viable), while the treated cells are red (dead with damaged cell membrane). The results from these relatively simple tests clearly demonstrate the major damages of visible light-activated CDots to the bacterial cell membrane and associated functionalities.

Mechanistically on the correlation of photoinduced antibacterial activities with optical properties and photoexcited state processes

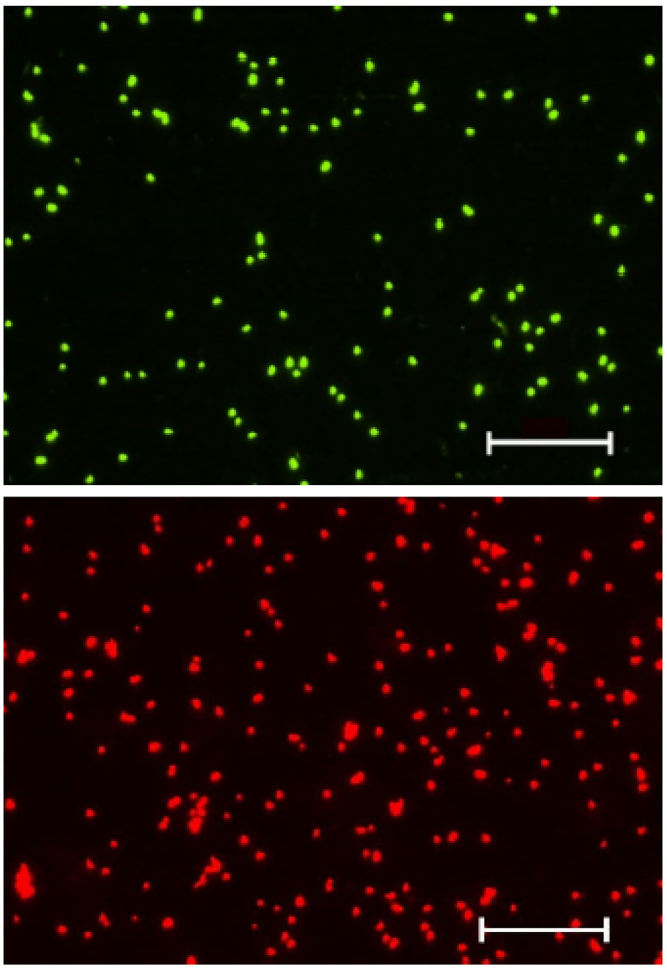

Fig. 7. Representative fluorescence images (50 μm for the scale bars) of BM46 cells after their being stained with the live/dead staining kit: (upper) cells in the control without the PEI-CDots treatment; and (lower) the cells treated with 1.2 μM_{DOTS} PEI-CDots under visible light for 1 h. (A colour version of this figure can be viewed online.)

of CDots, photodynamic effects as commonly found and understood in organic dye photosensitizers may represent a logical starting point. However, it should be emphasized that CDots, similar to other photoactive nanomaterials, are not simply fancy photosensitizers like organic dyes, but instead of fundamentally different characteristics from those of traditional organic molecular photosensitizers. First in terms of photon-harvesting, the optical absorptivities of CDots are orders of magnitude larger than those of organic dye molecules, thus enabling extremely effective and efficient light activation to drive the photoexcited state processes, including the classical photodynamic effects.

In the mechanistic framework for CDots in the photoexcited states, the initial ultrafast charge transfer and separation produce electrons and holes, which are trapped at the various passivated surface defect sites (Fig. 8). These separated redox pairs should be highly reactive, likely analogous to the charge separated species found in conventional semiconductor QDs following photoexcitation. According to the proposal by Courtney et al. [45], for example, there were "light-activated redox species" (LARS) in photoexcited CdTe QDs responsible for their observed bactericidal activities. One may draw parallels between the "LARS" in semiconductor QDs (or classically electron-hole pairs in the exciton model for nanoscale semiconductors) and the "separated electrons and holes" in CDots. In fact, the latter in PEI-CDots must be contributing substantially to

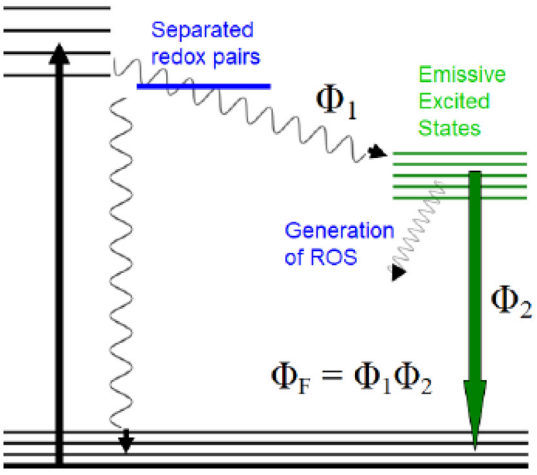

Fig. 8. A state energy diagram on the photoexcited states and processes of CDots, highligting the two sets of highly reactive species: the separated redox pairs from the initial charge transfer and separation; and the ROS generation as a part of the non-radiative deactivation of the emissive excited states. Φ_F denotes fluorescence quantum yields. (A colour version of this figure can be viewed online.)

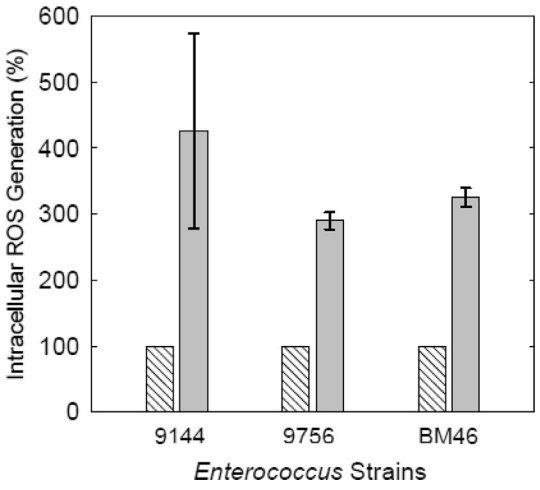

Fig. 9. The percentage increases in intracellular ROS generation in *Enterococcus* strains upon treatments with 1.2 μM_{DOTS} PEI-CDots under visible light for 1 h (grey bars, normalized against the controls in hatched bars as 100%).

the apparently highly potent antibacterial activities against the *Enterococcus* strains [46].

The likely ultrafast nature of the initial processes in the photoexcited CDots has been rather challenging to the desired direct experimental probing and analyses. Indirectly, the observed effective quenching of fluorescence emissions by both electron acceptors and donors has been considered as evidence for their "scavenging" the separated electrons and holes in CDots, respectively [9,16,47,48]. The same highly efficient fluorescence quenching of PEI-CDots was also found with the electron deficient 2,4-dinitrotoluene (DNT) and rich *N*,*N*-diethylaniline (DEA) molecules as quenchers at rather low concentrations (0.04 M and lower, for example) in ethanol, yielding Stern-Volmer quenching constants of 47 M^{-1} and 30 M^{-1}, respectively. Like those of many other CDots, the fluorescence decays of PEI-CDots are generally non-exponential, but can be deconvoluted with a bi-exponential function. The average fluorescence lifetime thus obtained for the PEI-CDots sample in this study was about 5 ns. Thus, the estimated diffusion rate constants for the quenchers DNT and DEA are 9.4×10^9 $M^{-1}s^{-1}$ and 6×10^9 $M^{-1}s^{-1}$, respectively, suggesting that the quenching was at or beyond the upper limit of diffusion control, with the "beyond" due to some near-neighbor (thus limited diffusion) interactions of quencher molecules with the photoexcited CDots (or "static quenching") [48].

The formation of emissive excited states (Fig. 8) may be considered as being similar to the radiative recombination of electron-hole pairs in the exciton model for semiconductor QDs. According to results from fluorescence decay measurements, the emissive excited states of CDots generally have short rising times of less than 200 ps but long decay times in nanoseconds [32], so that these states are more comparable with those commonly found in organic dye photosensitizers. Since the latter are known for photodynamic effects, with the generated reactive oxygen species (ROS) killing cancer cells in therapies or inactivating microbials for disinfections, the similarly generated ROS via the emissive excited states of CDots may be credited for contributions to the observed antibacterial actions. Experimentally, the presence of ROS in the *Enterococcus* cells treated with PEI-CDots under visible light was confirmed and quantified by using the established probe dihydrorhodamine 123 (DHR 123) [49,50]. The probe can enter the cells and upon the oxidation by ROS convert to rhodamine 123, a brightly fluorescent dye that is positively charged, hydrophobic, and accumulating in the mitochondria [49,50]. As shown in Fig. 9, the intracellular ROS levels thus determined in the treated cells were 3–4 times of those in the untreated controls.

The substantial presence of ROS in the treated cells validates their expected contributions to the observed antibacterial outcomes, though the role of the initial separated redox pairs in the photoexcited CDots (similar to the proposed LARS in some conventional semiconductor QDs) [45] may also be critical, as discussed above, namely that it must be the combination of all these reactive species responsible for the observed highly potent antibacterial activities. One may even expand the definition of ROS generated in photoexcited CDots to include the initially formed electrons and holes. However, these separated and trapped redox pairs (Fig. 8) are short lived, so that their actions must be near-neighbor in nature, conceptually and practically similar to the static fluorescence quenching discussed above. For PEI-CDots, their being in close proximity to the targeted bacterial cells for the near-neighbor requirement may have been facilitated by the positive charges on the dot surface (due to the abundant amine moieties in PEI at close to neutral pH), which are attracted to the negatively charged bacterial surface [25]. Because of the near-neighbor (limited diffusion) static quenching-like characteristics, the antibacterial action of the initial separated redox pairs can not be quenched with molecules commonly employed to scavenge the ROS generated by conventional organic photosensitizers, as confirmed by results from the scavenging experiments.

The BM46 strain was selected for the comparison between the treatments of light-activated PEI-CDots without and with the presence of the popular ROS scavenger L-histidine [51,52]. As shown in Fig. 10, the viable cell numbers decreased from the starting 2.3×10^8 CFU/mL to 2.4×10^4 CFU/mL (99.99% reduction) or 1.3×10^7 CFU/mL (~94% reduction) in the absence or presence of L-histidine, respectively, suggesting that the scavenger could provide some meaningful yet rather limited protection of the BM46 cells from the action of light-activated PEI-CDots. On the other hand, the decrease in the intracellular ROS level from without to with the presence of L-histidine in the treatment of the cells by light-activated PEI-CDots was much more substantial (by more than 50%, Fig. 10). The results are consistent with the notion discussed above that the highly effective and efficient antibacterial outcomes must be due to a combination of two different kinds of

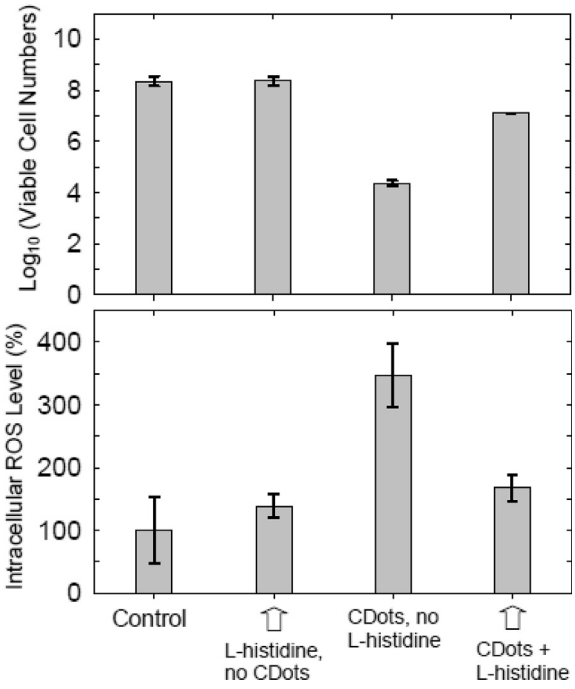

Fig. 10. Effects of the common ROS scavenger L-histidine (30 mM) in treatments of BM46 cells with 1.2 μM_{DOTS} PEI-CDots under visible light for 1 h: (upper) on the protection of the cells from inactivation in terms of viable cell reduction (CFU/mL) in log_{10} scale; and (lower) on the intracellular ROS generation.

reactive species produced in the photoexcited CDots, namely the separated redox pairs and the "classical" ROS. The latter could be scavenged by L-histidine, but more quantitatively the former seemed to contribute more to the observed inactivation.

The commonly used hydroxyl radical scavenger *t*-butanol was similarly evaluated, but no meaningful protective effect on the treated cells was found. A plausible explanation might be due to the short-lived nature of hydroxyl radicals in the aqueous medium.

The results presented and discussed above clearly show that photoexcited CDots are highly effective and efficient antibacterial agents, and PEI-CDots in particular are capable of inactivating completely the antibiotics-resistant *Enterococcus* strains, which are often considered as being among the toughest for any disinfection strategies [53–55]. On performance, CDots compare very favorably with conventional semiconductor QDs, and in addition, they offer a number of other major advantages including especially their benign and nontoxic nature [3], without the widely acknowledged heavy metal issues associated with semiconductor QDs. Interestingly, however, while CDots are hardly "quantum" for the lack of the classical quantum confinement effect that defines QDs, they apparently share both phenomenological and mechanistic features with conventional semiconductor QDs in photoinduced antimicrobial functions. Semiconductor QDs and CDots are both highly photoactive, but hardly more absorptive equivalents of organic dye molecules or polymers; and upon photoexcitation they both produce extremely reactive redox species, the LARS in QDs (CdTe, for example) [45] and the rather similar trapped electrons and holes in CDots (Fig. 8), whose contributions are credited for the observed more robust antimicrobial outcomes with both semiconductor QDs and CDots. Thus, what make QDs and CDots so special in the competition with classical dye photosensitizers for microbicidal effects are their enormous optical absorptivities for photon-harvesting and their generation of the extremely reactive redox species unique to the nanomaterials. In this regard, CDots are advantaged by their ready activation with visible/natural light and the benign and nontoxic nature. The available experimental results also seem to suggest more effective antimicrobial actions by CDots due to their initially formed redox species following photoexcitation, for which more experimental and theoretical investigations are needed and will prove very insightful and rewarding.

It should also be recognized that there have been many studies of various dot samples prepared by carbonizing organic precursors under different processing conditions, whose chemical compositions and structures may be significantly different from those of the CDots (Fig. 1) used in this investigation. Their reported antibacterial activities could have different mechanisms or mechanistic details [14,26–30]. A more global understanding of the shared mechanistic features in the light-activated microbicidal functions among the samples that all contain nanoscale carbon particles or domains and organic moieties but in different compositions, structures, and/or configurations remains an interesting challenge. For such a challenge, more comprehensive and quantitative characterizations of the different dot samples are necessary, and more specifically as suggested by one of the reviewers on the photodynamic effects, systematic photochemical investigations on the photosensitization behaviors and outcomes of the various dot samples are needed. Moreover, in light of the apparently dominating role of the separated and trapped redox pairs in the photoinduced antibacterial activities of CDots, more ultrafast spectroscopy experiments for the probing and analysis of the related transient species and processes are in demand.

4. Conclusions

CDots with the same strong optical absorptions as those of small carbon nanoparticles in the dot cores are excellent in harvesting visible photons. Upon the photoexcitation, there are rapid charge transfer and separation for the formation of electrons and holes, which are likely trapped at various surface defect sites stabilized by the passivation due to dot surface organic functionalization. These separated redox pairs are credited for their major contributions to the observed antibacterial activities, and such contributions can not be quenched by ROS scavengers commonly used in the study of photodynamic effects with classical molecular photosensitizers. Thus, what make CDots uniquely effective and efficient visible/natural light-activated antimicrobial agents are their large absorptivities over the visible spectrum and the photo-generated highly reactive redox species. The latter may be incorporated into a broader mechanistic framework on CDots for photodynamic inactivation of microbials. It is hoped that the results and discussion will stimulate interests in the development of solid state physics theories for the more precise elucidation of growing experimental data beyond simple evident-based speculations.

CRediT authorship contribution statement

Xiuli Dong: Investigation, Supervision. **Lin Ge:** Investigation. **Dina I. Abu Rabe:** Investigation. **Oluwayemisi O. Mohammed:** Investigation. **Ping Wang:** Investigation. **Yongan Tang:** Investigation. **Sophia Kathariou:** Supervision. **Liju Yang:** Conceptualization, Supervision, Writing - original draft. **Ya-Ping Sun:** Conceptualization, Supervision, Writing - original draft.

Declaration of competing interest

The authors declare that they have no known competing financial interests or personal relationships that could have appeared to influence the work reported in this paper.

Acknowledgment

Financial support from NSF (1701399, 1701424, and 1855905) and USDA (2019-67018-29689) is gratefully acknowledged.

Appendix A. Supplementary data

Supplementary data to this article can be found online at https://doi.org/10.1016/j.carbon.2020.08.025.

References

[1] Y.-P. Sun, B. Zhou, Y. Lin, W. Wang, K.A.S. Fernando, P. Pathak, M.J. Meziani, B.A. Harruff, X. Wang, H. Wang, et al., Quantum-sized carbon dots for bright and colorful photoluminescence, J. Am. Chem. Soc. 128 (2006) 7756–7757.
[2] Y.-P. Sun, Fluorescent carbon nanoparticles, U.S. Patent 7 (2010), 829,772.
[3] Y.-P. Sun, Carbon Dots - Exploring Carbon at Zero-Dimension, Springer International Publishing, 2020.
[4] L. Cao, M.J. Meziani, S. Sahu, Y.-P. Sun, Photoluminescence properties of graphene versus other carbon nanomaterials, Acc. Chem. Res. 46 (2013) 171–180.
[5] P.G. Luo, S. Sahu, S.-T. Yang, S.K. Sonkar, J. Wang, H. Wang, G.E. LeCroy, L. Cao, Y.-P. Sun, Carbon “quantum” dots for optical bioimaging, J. Mater. Chem. B 1 (2013) 2116–2127.
[6] C. Ding, A. Zhu, Y. Tian, Functional surface engineering of C-dots for fluorescent biosensing and in vivo bioimaging, Acc. Chem. Res. 47 (2014) 20–30.
[7] S.Y. Lim, W. Shen, Z. Gao, Carbon quantum dots and their applications, Chem. Soc. Rev. 44 (2015) 362–381.
[8] V. Georgakilas, J.A. Perman, J. Tucek, R. Zboril, Broad family of carbon nanoallotropes: classification, chemistry, and applications of fullerenes, carbon dots, nanotubes, graphene, nanodiamonds, and combined superstructures, Chem. Rev. 115 (2015) 4744–4822.
[9] K.A.S. Fernando, S. Sahu, Y. Liu, W.K. Lewis, E.A. Guliants, A. Jafariyan, P. Wang, C.E. Bunker, Y.-P. Sun, Carbon quantum dots and applications in photocatalytic energy conversion, ACS Appl. Mater. Interfaces 7 (2015) 8363–8376.
[10] G.E. LeCroy, S.-T. Yang, F. Yang, Y. Liu, K.A.S. Fernando, C.E. Bunker, Y. Hu, P.G. Luo, Y.-P. Sun, Functionalized carbon nanoparticles: syntheses and applications in optical bioimaging and energy conversion, Coord. Chem. Rev. 320 (2016) 66–81.
[11] G.A.M. Hutton, B.C.M. Martindale, E. Reisner, Carbon dots as photosensitisers for solar-driven catalysis, Chem. Soc. Rev. 46 (2017) 6111–6123.
[12] P. Namdari, B. Negahdari, A. Eatemadi, Synthesis, properties and biomedical applications of carbon-based quantum dots: an updated review, Biomed. Pharmacother. 87 (2017) 209–222.
[13] J. Du, N. Xu, J. Fan, W. Sun, X. Peng, Carbon dots for in vivo bioimaging and theranostics, Small 15 (2019) 1805087.
[14] X. Dong, W. Liang, M.J. Meziani, Y.-P. Sun, L. Yang, Carbon dots as potent antimicrobial agents, Theranostics 10 (2020) 671–686.
[15] W. Liang, C.E. Bunker, Y.-P. Sun, Carbon dots: zero-dimensional carbon allotrope with unique photoinduced redox characteristics, ACS Omega 5 (2020) 965–971.
[16] L. Cao, K.A.S. Fernando, W. Liang, A. Seilkop, L.M. Veca, Y.-P. Sun, C.E. Bunker, Carbon dots for energy conversion applications, J. Appl. Phys. 125 (2019) 220903.
[17] L. Cao, P. Anilkumar, X. Wang, J.-H. Liu, S. Sahu, M.J. Meziani, E. Myers, Y.-P. Sun, Reverse stern-volmer behavior for luminescence quenching in carbon nanoparticles, Can. J. Chem. 89 (2011) 104–109.
[18] T. Yuan, T. Meng, P. He, Y. Shi, Y. Li, X. Li, L. Fan, S. Yang, Carbon quantum dots: an emerging material for optoelectronic applications, J. Mater. Chem. C 7 (2019) 6820–6835.
[19] L. Yan, Y. Yang, C.-Q. Ma, X. Liu, H. Wang, B. Xu, Synthesis of carbon quantum dots by chemical vapor deposition approach for use in polymer solar cell as the electrode buffer layer, Carbon 109 (2016) 598–607.
[20] B. Cui, L. Yan, H. Gu, Y. Yang, X. Liu, C.-Q. Ma, Y. Chen, H. Jia, Fluorescent carbon quantum dots synthesized by chemical vapor deposition: an alternative candidate for electron acceptor in polymer solar cells, Opt. Mater. 75 (2018) 166–173.
[21] X. Zhang, Y. Zhang, Y. Wang, S. Kalytchuk, S.V. Kershaw, Y. Wang, P. Wang, T. Zhang, Y. Zhao, H. Zhang, et al., Color-switchable electroluminescence of carbon dot light-emitting diodes, ACS Nano 7 (2013) 11234–11241.
[22] L. Cao, S. Sahu, P. Anilkumar, C.E. Bunker, J. Xu, K.A.S. Fernando, P. Wang, E.A. Guliants, K.N. Tackett, Y.-P. Sun, Carbon nanoparticles as visible-light photocatalysts for efficient CO_2 conversion and beyond, J. Am. Chem. Soc. 133 (2011) 4754–4757.
[23] M.J. Meziani, X. Dong, L. Zhu, L.P. Jones, G.E. LeCroy, F. Yang, S. Wang, P. Wang, Y. Zhao, L. Yang, et al., Visible-light-activated bactericidal functions of carbon “quantum” dots, ACS Appl. Mater. Interfaces 8 (2016) 10761–10766.
[24] M.M. Al Awak, P. Wang, S. Wang, Y. Tang, Y.-P. Sun, L. Yang, Correlation of carbon dots' light-activated antimicrobial activities and fluorescence quantum yield, RSC Adv. 7 (2017) 30177–30184.
[25] D.I. Abu Rabe, M.M. Al Awak, F. Yang, P.A. Okonjo, X. Dong, L.R. Teisl, P. Wang, Y. Tang, N. Pan, Y.-P. Sun, et al., The dominant role of surface functionalization in carbon dots' photo-activated antibacterial activity, Int. J. Nanomed. 14 (2019) 2655–2665.
[26] M. Kováčová, Z.M. Marković, P. Humpolíček, M. Micusik, H. Švajdlenková, A. Kleinova, M. Danko, P. Kubát, J. Vajďák, Z. Capáková, M. Lehocký, L. Münster, B.M. Todorović-Marković, Z. Spitalsky, Carbon quantum dots modified polyurethane nanocomposite as effective photocatalytic and antibacterial agents, ACS Biomater. Sci. Eng. 4 (2018) 3983–3993.
[27] S.R. Anand, A. Bhati, D. Saini, Gunture, N. Chauhan, P. Khare, S.K. Sonkar, Antibacterial nitrogen-doped carbon dots as a reversible “fluorescent nanoswitch” and fluorescent ink, ACS Omega 4 (2019) 1581–1591.
[28] Z.M. Marković, M. Kováčová, P. Humpolíček, M.D. Budimir, J. Vajdák, P. Kubát, M. Micusik, H. Švajdlenková, M. Danko, Z. Capáková, M. Lehocký, B.M. Todorović-Marković, Z. Spitalsky, Antibacterial photodynamic activity of carbon quantum dots/polydimethylsiloxane nanocomposites against *Staphylococcus aureus, Escherichia coli* and *Klebsiella pneumoniae*, Photodiagnosis Photodyn. Ther. 26 (2019) 342–349.
[29] T.G. Chatzimitakos, A.I. Kasouni, A.N. Troganis, C.D. Stalikas, Exploring the antibacterial potential and unraveling the mechanism of action of non-doped and heteroatom-doped carbon nanodots, J. Nanoparticle Res. 22 (2020) 36.
[30] M. Kováčová, E. Špitalská, Z. Markovic, Z. Špitálský, Carbon quantum dots as antibacterial photosensitizers and their polymer nanocomposite applications, Part. Part. Syst. Char. 37 (2020) 1900348.
[31] F. Yang, G.E. LeCroy, P. Wang, W. Liang, J. Chen, K.A.S. Fernando, C.E. Bunker, H. Qian, Y.-P. Sun, Functionalization of carbon nanoparticles and defunctionalization-toward structural and mechanistic elucidation of carbon “quantum” dots, J. Phys. Chem. C 120 (2016) 25604–25611.
[32] G.E. LeCroy, F. Messina, A. Sciortino, C.E. Bunker, P. Wang, K.A.S. Fernando, Y.-P. Sun, Characteristic excitation wavelength dependence of fluorescence emissions in carbon "quantum" dots, J. Phys. Chem. C 121 (2017) 28180–28186.
[33] A. Sciortino, A. Madonia, M. Gazzetto, L. Sciortino, E.J. Rohwer, T. Feurer, F.M. Gelardi, M. Cannas, A. Cannizzo, F. Messina, The interaction of photoexcited carbon nanodots with metal ions disclosed down to the femtosecond scale, Nanoscale 9 (2017) 11902–11911.
[34] A. Sciortino, M. Gazzetto, M.L. Soriano, M. Cannas, S. Cárdenas, A. Cannizzo, F. Messina, Ultrafast spectroscopic investigation on fluorescent carbon nanodots: the role of passivation, Phys. Chem. Chem. Phys. 21 (2019) 16459–16467.
[35] P. Kambhampati, Unraveling the structure and dynamics of excitons in semiconductor quantum dots, Acc. Chem. Res. 44 (2011) 1–13.
[36] J.S. Kim, E. Kuk, K.N. Yu, J.-H. Kim, S.J. Park, H.J. Lee, S.H. Kim, Y.K. Park, Y.H. Park, C.-Y. Hwang, et al., Antimicrobial effects of silver nanoparticles, Nanomed.- Nanotechnol. 3 (2007) 95–101.
[37] H. Yin, L. Xu, N.A. Porter, Free radical lipid peroxidation: mechanisms and analysis, Chem. Rev. 111 (2011) 5944–5972.
[38] A.W. Girotti, Lipid hydroperoxide generation, turnover, and effector action in biological systems, J. Lipid Res. 39 (1998) 1529–1542.
[39] J. Kanner, J.B. German, J.E. Kinsella, H.O. Hultin, Initiation of lipid peroxidation in biological systems, Crit. Rev. Food Sci. Nutr. 25 (1987) 317–364.
[40] H. Esterbauer, K.H. Cheeseman, M.U. Dianzani, G. Poli, T.F. Slater, Separation and characterization of the aldehydic products of lipid peroxidation stimulated by ADP-Fe^{2+} in rat liver microsomes, Biochem. J. 208 (1982) 129–140.
[41] H. Esterbauer, R.J. Schaur, H. Zollner, Chemistry and biochemistry of 4-hydroxynonenal, malonaldehyde and related aldehydes, Free Radical Biol. Med. 11 (1991) 81–128.
[42] R.O. Sinnhuber, T.C. Yu, Characterization of the red pigment formed in the 2-thiobarbituric acid determination of oxidative rancidity, J. Food Sci. 7 (1958) 626–634.
[43] H. Esterbauer, K.H. Cheeseman, Determination of aldehydic lipid peroxidation products: malonaldehyde and 4-hydroxynonenal, Methods Enzymol. 186 (1990) 407–421.
[44] W.A. Pryor, On the detection of lipid hydroperoxides in biological samples, Free Radical Biol. Med. 7 (1989) 177–178.
[45] C.M. Courtney, S.M. Goodman, J.A. McDaniel, N.E. Madinger, A. Chatterjee, P. Nagpal, Photoexcited quantum dots for killing multidrug-resistant bacteria, Nat. Mater. 15 (2016) 529–534.
[46] D.I. Abu Rabe, O.O. Mohammed, X. Dong, A.K. Patel, C.M. Overton, Y. Tang, S. Kathariou, Y.-P. Sun, L. Yang, Carbon dots for highly effective photodynamic inactivation of multidrug-resistant bacteria, Mater. Adv. 1 (2020) 321–325.
[47] X. Wang, L. Cao, F. Lu, M.J. Meziani, H. Li, G. Qi, B. Zhou, B.A. Harruff, Y.-P. Sun, Photoinduced electron transfers with carbon dots, Chem. Commun. (2009) 3774–3776.
[48] G.E. LeCroy, K.A.S. Fernando, C.E. Bunker, P. Wang, N. Tomlinson, Y.-P. Sun, Steady-state and time-resolved fluorescence studies on interactions of carbon "quantum" dots with nitrotoluenes, Inorg. Chim. Acta. 468 (2017) 300–307.
[49] S.E. Buxser, G. Sawada, T.J. Raub, Analytical and numerical techniques for evaluation of free radical damage in cultured cells using imaging cytometry and fluorescent indicators, Methods Enzymol. 300 (1999) 256–275.
[50] F. Petrat, S. Pindiur, M. Kirsch, H. de Groot, NAD(P)H, A primary target of $^1O_2$ in mitochondria of intact cells, J. Biol. Chem. 278 (2003) 3298–3307.
[51] K. Hara, S. Holland, J. Woo, Effects of exogenous reactive oxygen species scavengers on the survival of Escherichia coli B23 during exposure to UV-A radiation, J. Exp. Microbiol. Immunol. 12 (2004) 62–66.
[52] K. Ishiyama, K. Nakamura, H. Ikai, T. Kanno, M. Kohno, K. Sasaki, Y. Niwano,

Bactericidal action of photogenerated singlet oxygen from photosensitizers used in plaque disclosing agents, PloS One 7 (2012), e37871.
[53] M.M. Huycke, D.F. Sahm, M.S. Gilmore, Multiple-drug resistant enterococci: the nature of the problem and an agenda for the future, Emerg. Infect. Dis. 4 (1998) 239–249.
[54] B.L. Hollenbeck, L.B. Rice, Intrinsic and acquired resistance mechanisms in Enterococcus, Virulence 3 (2012) 421–433.
[55] W.R. Miller, J.M. Munita, C.A. Arias, Mechanisms of antibiotic resistance in enterococci, Expert Rev. Anti Infect. Ther. 12 (2014) 1221–1236.